# Comparing the low-frequency content of seismic source-receiver combinations using surface-wave analysis: A field case from Hussar, Alberta

Yu-Tai Wu and Robert R. Stewart

Allied Geophysical Laboratories

## ABSTRACT

The low-frequency content in seismic exploration is crucial as it can benefit imaging and inversion by providing broader-band energy, wavelet stability, and higher resolution. However, the low-frequency content of source and receiver types is often uncertain and requires evaluation. The Hussar, Alberta survey, conducted by the CREWES Project, addressed this purpose. We further assess the low-frequency content of its data sets using surface-wave analysis. The survey tested 2 kg dynamite in addition to vibroseis sources with linear and low-dwell sweeps. The receivers tested included Vectorseis accelerometers, 10 Hz, and 4.5 Hz geophones. Our dispersion inversion results indicate that all source-receiver combinations can provide a reasonable Vs model, which fits well with S-wave tomography and well-log measurements. Regarding the evaluation results, dynamite exhibited the most pronounced low-frequency energy, while low-dwell sweeps showed more clear low-frequency signals than the linear sweep. Among the tested receivers, the 4.5 Hz geophone demonstrated the most optimal performance. When considering the lowest frequency a receiver can measure, the Vectorseis accelerometer outperformed the 10 Hz geophone. Using the energy and coherency of surface-wave analysis to access low-frequency content can complement other types of spectral analysis.

## METHODS

**Dispersion curve calculation (NLSC method)**

Multi-channel results stacked using the results of i-th and j-th traces:

$$S'_{MNLSC}(\omega, V_{ph}, \sigma) = \sum_{i=1}^{n-1} \sum_{j=1+i}^{n} \frac{S_{NL}^{ij}(\omega, V_{ph}, \sigma) - S_\pi}{1 - S_\pi}$$

Angular frequency | Phase velocity | Resolution controlling parameter

$S_{NL}$ and $S_\pi$ are the normalized dispersion map and a background value for normalization, respectively.

$$S_{NL}(\omega, V_{ph}, \sigma) = \frac{1}{T} \int_0^T \exp\left\{ -\frac{\left[\bar{d}_1(t,\omega) - \bar{d}_x(t + \frac{x}{V_{ph}}, \omega)\right]^2}{4\sigma^2 \omega^2 x^{-2}} \right\}^2 dt$$

Time window | Seismic data | Receiver Spacing

$$S_\pi(\omega, \sigma) = I_0(b) e^{-b}, b = \frac{\pi^2}{\sigma^2 \omega^2 T}$$

Modified zeroth-order Bessel function

(Zheng and Hu, 2017)

**Modeling and inversion of dispersion curves**

**(Thin-bed method)**

$$\begin{bmatrix} \boldsymbol{I} & 0 \\ 0 & \boldsymbol{B}_2 \end{bmatrix} \begin{bmatrix} \boldsymbol{v} \\ \boldsymbol{\alpha} \end{bmatrix} = \begin{bmatrix} 0 & \boldsymbol{I} \\ \omega^2 \boldsymbol{M} - \boldsymbol{B}_0 & -\boldsymbol{B}_1 \end{bmatrix} \begin{bmatrix} \boldsymbol{v} \\ \boldsymbol{\alpha} \end{bmatrix}$$

Stiffness matrices | Mass matrix | Nodal displacements

At fixed frequency, the perturbation in phase velocity caused by model perturbations can be represented as

$$\frac{\delta V_{ph}}{V_{ph}} = \frac{1}{2k^2 U V_{ph} \boldsymbol{v}^T \boldsymbol{M} \boldsymbol{v}} \sum_{i=1}^{N} \left( \begin{array}{l} \boldsymbol{v}^T \frac{\partial (k^2 \boldsymbol{B}_2 + k \boldsymbol{B}_1 + \boldsymbol{B}_0)}{\partial \mu_i} \boldsymbol{v} \partial \mu_i \\ + \boldsymbol{v}^T \frac{\partial (k^2 \boldsymbol{B}_2 + k \boldsymbol{B}_1 + \boldsymbol{B}_0)}{\partial \lambda_i} \boldsymbol{v} \partial \lambda_i \\ - \omega^2 \boldsymbol{v}^T \frac{\partial \boldsymbol{M}}{\partial \rho_i} \boldsymbol{v} \partial \rho_i \end{array} \right)$$

Shear modulus | Lame's constant | Density

$$U = \frac{\delta \omega}{\delta k} = \frac{\boldsymbol{v}^T (2k \boldsymbol{B}_2 + \boldsymbol{B}_1) \boldsymbol{v}}{2\omega \boldsymbol{v}^T \boldsymbol{M} \boldsymbol{v}}$$

Group velocity

(Haney and Tsai , 2017)

## Area of study and input data

The research dataset used in this study was obtained from a seismic experiment conducted by the CREWES Project in collaboration with Husky Energy, Geokinetics, and INOVA. The primary objective of the experiment was to study low-frequency seismic reflections and test inversion methods. The dataset comprises recordings from a 4.5 km multi-component seismic line near Hussar.

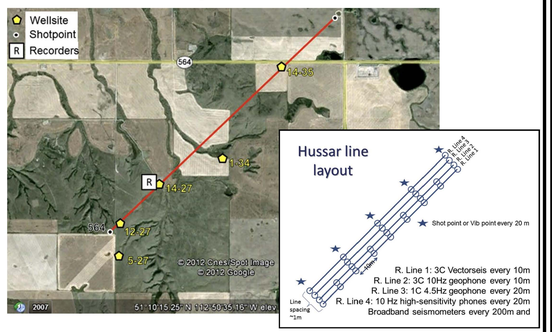


Map view of the Hussar seismic line shown with 5 wells. Only well 12-27 has shear velocity measurements

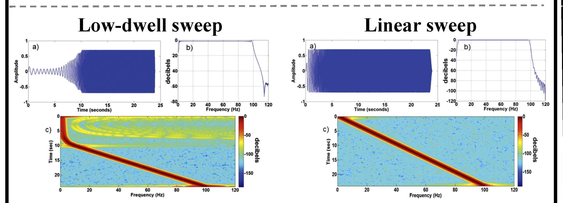


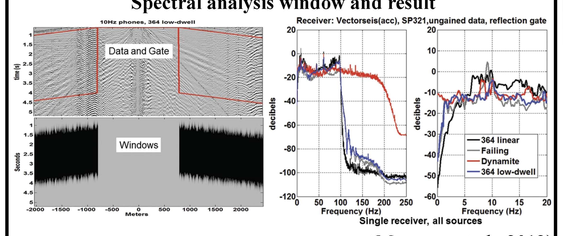


(Margrave et al., 2012)

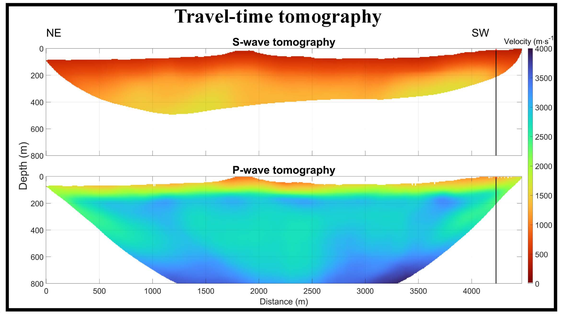


## Dispersion maps

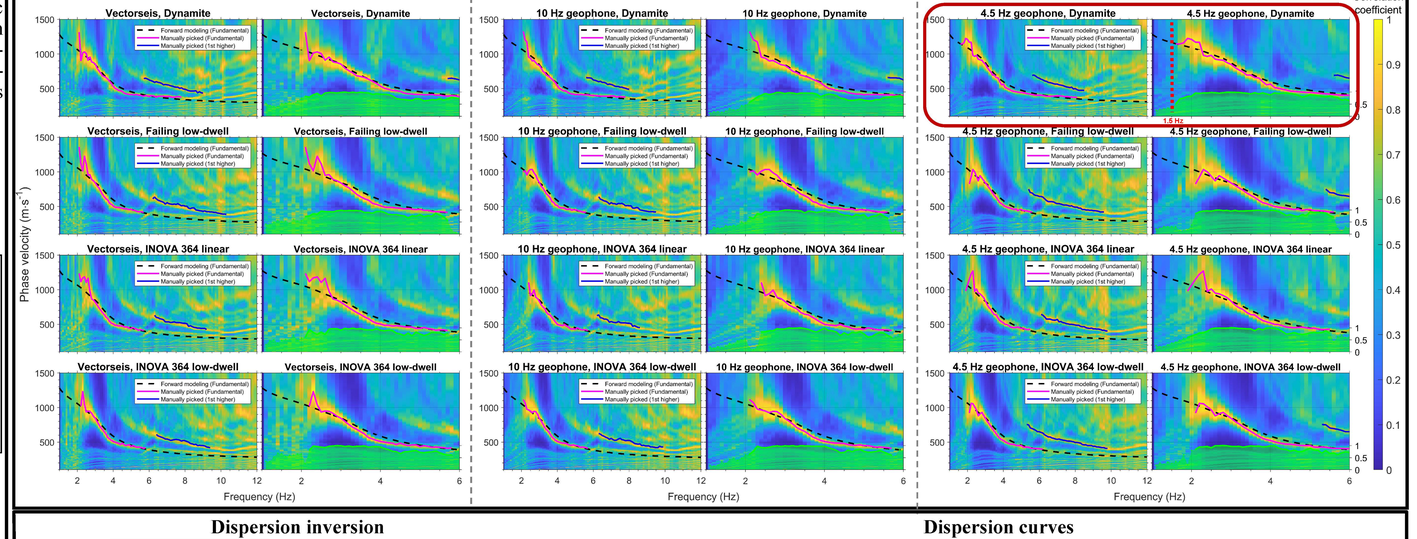


## Dispersion inversion

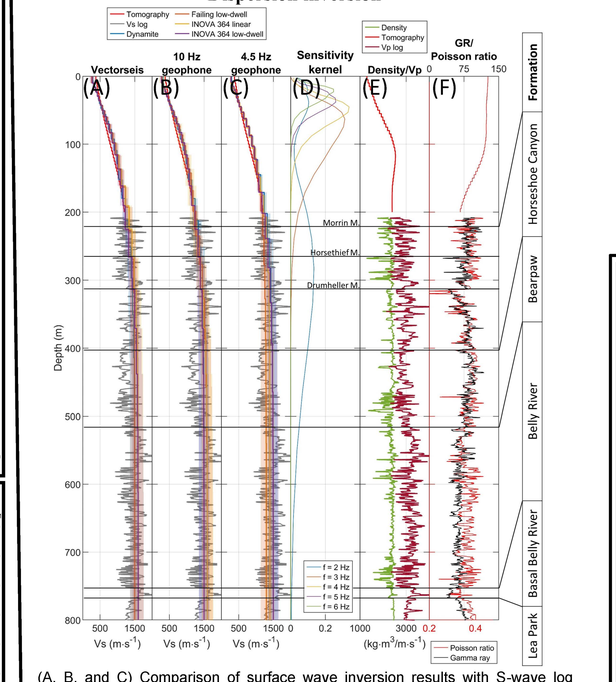


(A, B, and C) Comparison of surface wave inversion results with S-wave log measurements and tomography model. (D) Sensitivity kernels of 2- to 6-Hz surface waves. (E) Acoustic and density logs are shown along with Vp from the tomography model in Figure 7. (F) Gamma-ray log plotted with Poisson ratio calculated from velocities of log measurements and tomography models. Corresponding formation tops at the study site are shown on the right.

## Dispersion curves

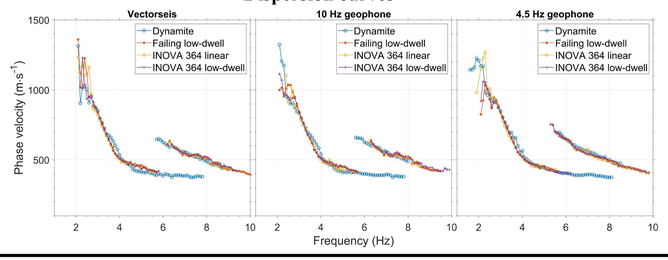


## CONCLUSIONS

1. A valuable case study for characterizing near-surface properties through surface-wave analysis using low-frequency data down to 1.5 Hz .
2. Among all source types, dynamite exhibited the strongest low-frequency energy. The type of sweep function had a more significant impact than the vibrator type. The two low-dwell sweeps were nearly identical in terms of dispersion curves and displayed more pronounced low-frequency signals compared to the linear sweep.
3. The 4.5 Hz geophone performed the best in displaying low frequencies. When considering the lowest frequency a receiver can record, the Vectorseis accelerometer outperformed the 10 Hz geophone. However, interpreted instrument noise of Vectorseis accelerometers may impact data in the low-frequency range.

## ACKNOWLEDGEMENTS

The authors express their appreciation to the CREWES Project, in particular. Dr. Kris Innanen, and its sponsors for providing the Hussar data set for our research. We also thank the Hewlett Packard Enterprise Data Science Institute at the University of Houston for providing computing

## REFERENCES

Haney, M. M., and Tsai, V. C., 2017, Perturbational and nonperturbational inversion of Rayleigh-wave velocities: Geophysics, 82, F15–F28.

Margrave, G. F., Mewhort, L., Phillips, T., Hall, M., Bertram, M. B., Lawton, D. C., Innanen, K., Hall, K. W., and Bertram, K., 2012, The Hussar low-frequency experiment: CSEG Recorder, 37, 25–39.

Zheng, Y., and Hu, H., 2017, Nonlinear signal comparison and high-resolution measurement of surface wave dispersion: Seismol. Soc. Am., 107, 1551–1556.